Charm hadron azimuthal angular correlations in Au + Au collisions at $\sqrt{s_{\mathrm{NN}}} = 200$ GeV from parton scatterings

Hai Wang[1,2] · **Jin-Hui Chen**[3] · **Yu-Gang Ma**[1,3] · **Song Zhang**[3]

Abstract The dynamic evolution of the charm hadron in hot quark matter was studied in the framework of a multiphase transport (AMPT) model. We first reproduced the open charm hadron $D_0 p_{\mathrm{T}}$ spectrum in Au + Au collisions at $\sqrt{s_{\mathrm{NN}}} = 200$ GeV by triggering the $c\bar{c}$ production in AMPT, and then the elliptic flow of charm hadrons was described with different parton cascade cross sections. Charm hadron azimuthal angular correlations were proposed, and they are affected by the different parton cross-section parameter applied in the model, which can facilitate our understanding of the loss of collision energy of charm quarks in hot quark medium and can stimulate further experimental studies.

Keywords Quark gluon plasma · Heavy flavor · Two-particle correlations

✉ Jin-Hui Chen
chenjinhui@fudan.edu.cn

1 Shanghai Institute of Applied Physics, Chinese Academy of Sciences, Shanghai 201800, China

2 University of Chinese Academy of Sciences, Beijing 100049, China

3 Institute of Modern Physics and Key Laboratory of Nuclear Physics and Ion-beam Application (MOE), Fudan University, Shanghai 200433, China

1 Introduction

Heavy flavor hadrons are important in the studies of the properties of quark–gluon plasma (QGP), which is believed to be created in ultrarelativistic heavy ion collisions [1–3]. The energy–momentum scale of hard probes is sufficiently large to enable the calculation of their initial production rate, the medium modification of the final spectra, and the correlations at high transverse momentum p_{T} based on perturbative quantum chromodynamics (pQCD). These hard probes can provide valuable information on the hot QCD medium. It is suggested that in heavy ion collisions at the relativistic heavy ion collider (RHIC) and at the large hadron collider (LHC), the massive heavy quarks undergo Brownian-like motion at low momentum, which provide information on the hadronization mechanisms at intermediate momentum, and merge into a radiative energy loss regime at high momentum [4, 5]. Therefore, to study heavy quarks, the spectral modification can be used, which results from the interactions between the heavy and light quarks and gluons propagating in their dynamically evolving QCD medium [5–7].

The heavy flavor quarks have mass effects, which enable systematic investigations of the variation of the prevalent processes in different p_{T} regions. Compared with light quarks and gluons, the large mass of heavy flavor quarks suppresses the small angle gluon radiation, which results in smaller loss of radiated energy [5–7]. The large mass slows down the equilibration speed of the heavy flavor quarks through the medium relative to their light counterparts. Therefore, the non-equilibrated heavy flavor quarks in the final state can provide valuable information on their interaction with the medium throughout their propagation in the QGP medium. For example, charm quarks, with

significantly larger mass compared to that of light quarks, can achieve a strong collective flow when they diffuse through the QGP [8–11]. Experimentally, this scenario was first found in measurements of the semi-leptonic electron decay spectra at RHIC [12, 13], followed by its confirmation by charm quark collectivity measurements at both RHIC and LHC [12–14].

The interactions of heavy flavor with the medium can be illustrated by scattering on the medium partons. When hard-scattered partons diffuse through the QGP, they lose energy in the QGP medium. At high p_T, the mass effect diminishes and heavy flavor observables degenerate to light flavor. At low p_T, a dead-cone effect is expected to arise, which suggests an inverse mass dependence of the energy loss from heavy quarks to light quarks and to gluons [15]. However, the experimental data do not fully support this mechanism. The observations of the heavy flavor nuclear modification factor and elliptic flow are nearly comparable to those of light hadrons [16–19], which suggest the importance of the loss of elastic energy in the QGP. Heavy flavor hadrons are ideal for the systematic investigation of the relationship of the radiative and collisional energy loss mechanisms over a broad momentum region and for the identification of the transition between the two [20, 21]. In this study, we used a multiphase transport (AMPT) model [22] to investigate the dynamics of elastic scattering among partons to understand their propagation into the heavy flavor production and their evolution in the QGP medium. We introduced the $c\bar{c}$ trigger to enhance the charm quark rate in AMPT, in order to reproduce the open charm hadron p_T distributions in Au + Au collisions at $\sqrt{s_{NN}}$ = 200 GeV. Then, the charm hadron azimuthal angular correlations study was used to investigate the collision energy loss dynamics.

2 Method and results

2.1 The AMPT model

The AMPT model [22, 23] is a transport model consisting of four main components: initial conditions, partonic interactions, conversion from partonic to hadronic matter, and hadronic interactions. The initial conditions, with spatial and momentum distributions of minijet partons and soft string excitations included, are obtained from the heavy ion jet interaction generator (HIJING) model [24], which is an extension of the PYTHIA model [25]. A Woods–Saxon radial shape is used for the colliding gold nuclei, and a parameterized nuclear shadowing function that depends on the impact parameter of the collision [24] is introduced. Scatterings among partons are modeled by

Zhang's parton cascade (ZPC) [26], which at present, include only two-body elastic scatterings with cross sections obtained from pQCD with screening mass. In the default version of the AMPT model, after the partons stop interacting, they recombine with their parent strings, which are produced from initial soft nucleon–nucleon interactions. The resulting strings are converted to hadrons using the Lund string fragmentation model. However, in the case of the string melting version of AMPT model, the hadrons produced from string fragmentation are converted to their valence quarks and antiquarks. The subsequent partonic interactions are modeled by ZPC. Following the freeze-out of the partons, they are recombined into hadrons by a quark coalescence process. The dynamic evolution of the hadronic phase is subsequently described by an extended relativistic transport (ART) model [27] including baryon–baryon, baryon–meson, and meson–meson elastic and inelastic scatterings. Details of the AMPT model are found in Ref. [22].

2.2 Quark phase space and charm hadron p_T distributions in the AMPT model

As we focus on the parton scattering effect on charm hadron azimuthal angular correlation study, in the following, the string melting version of the AMPT model (v2.26t5) is employed [23]. In this version of ZPC, two partons undergo scattering every time when they approach each other with a distance smaller than $\sqrt{\sigma/\pi}$ and with a total parton elastic scattering cross section of $\sigma \approx 9\pi\alpha_s^2/(2\mu^2)$. This transport process in AMPT simulates the parton energy loss in hot QGP medium [22]. We set the strong coupling constant as $\alpha_s = 0.33$ and screening mass as $\mu = 2.265$/fm or 1.241/fm for $\sigma = 3$ mb or 10 mb, respectively [22]. Figure 1 shows the momentum space density of charm quarks together with light quarks and the corresponding charm hadrons in 0–80% Au + Au collisions at $\sqrt{s_{NN}}$ = 200 GeV from AMPT model. Figure 1a shows the quark rapidity density distributions, while Fig. 1b shows their transverse momentum spectrum distributions. The charm quarks density dN/dy at mid-rapidity is approximately 0.4, and the rapidity density of light quarks is close to 500.

We found that this charm quark density is significantly lower than the result at RHIC energies [18, 28]. To improve the prediction power, we enabled the $c\bar{c}$ trigger in HIJING [24] to enhance the total rate of $c\bar{c}$ in our study. The physical process of charm quark evolution is identical to that of other charm quarks in the model. The trigger rate is determined by the experimentally measured cross section. For example, to match the rate at RHIC, we randomly triggered half of the full event sample, and the mid-rapidity
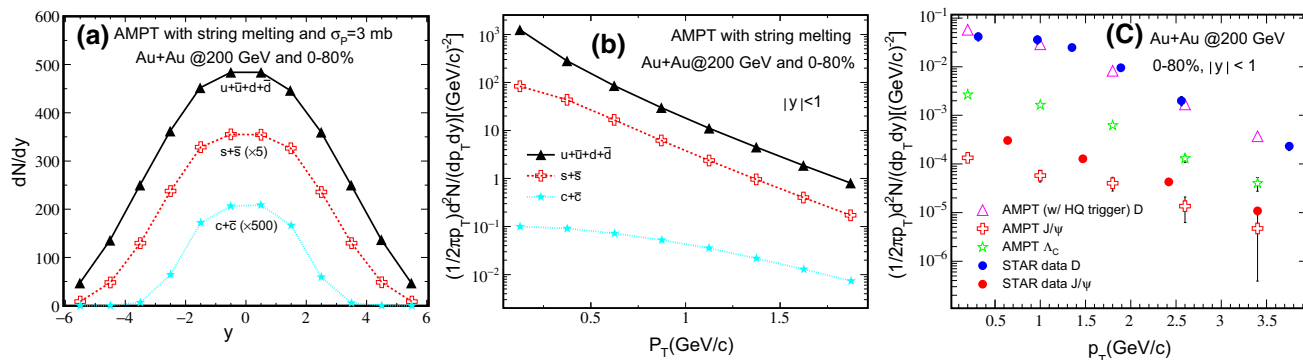
Fig. 1 (Color online) **a** Rapidity density of charm quarks $(c + \bar{c})$ and strange quarks $(s + \bar{s})$ as well as light quarks $(u + \bar{u} + d + \bar{d})$ at parton freeze-out in Au + Au collisions at $\sqrt{s_{NN}} = 200$ GeV. **b**, **c** p_T distributions, for quarks (**b**) and for the corresponding charm hadrons (**c**) compared with experimental data [18, 28]

density of charm quark reached ~ 3.6 in the 0–80% central Au + Au collisions at $\sqrt{s_{NN}} = 200$ GeV. The AMPT model with similar direction is currently under development [29].

As the inelastic scatterings among partons are not included in the current version of the AMPT model, the quarks produced from the melting of strings scatter uninterruptedly and then freeze out. Those freeze-out charm quarks coalescence with the nearby partons to form hadrons continue their evolution in the hadronic medium modeled by ART, and then freeze out, as shown in Fig. 1c. With the enhanced production of $c\bar{c}$ in the early stage of the AMPT process, the result of the D meson p_T spectrum from the AMPT model can reasonably reproduce the experimental data. However, the results from the $J/\psi p_T$ spectrum are lower than the data. This can be attributed to the fact, that there is no initial production and dissociation of J/ψ particles in the medium. A prediction for Λ_c is also presented, which can be found between Ds and J/ψs (cf. Fig. 1c).

Then, the history of charm quark interactions was analyzed in AMPT, by tracing the dynamics of parton cascading by the number of collisions ($N_{\text{scattering}}$) of one charm quark with other partons. The procedure described in Ref. [30] was strictly followed, but with a focus on the charm quarks. Figure 2a shows the probability distributions of the charm quarks freeze-out after $N_{\text{scattering}}$ collisions. In average, partons are subjected to $\langle N_{\text{scattering}} \rangle = 4$–5 Au + Au collisions at $\sqrt{s_{NN}} = 200$ GeV with $\sigma = 3$ mb and impact parameter $b = 8$ fm, while the number becomes 8–9 for $\sigma = 10$ mb. As shown in Fig. 2b, the average elastic energy loss of a charm quark with p_T is close to 2 GeV/c. The charm quarks continuously lose energy due to the two-body elastic scattering in ZPC. The $\langle \Delta E \rangle$ is the largest in the first collision; it drops gradually as more collisions occur, and apparently, it stabilizes with larger $\langle N_{\text{scattering}} \rangle$. It is understood that the $\langle \Delta E \rangle$ is smaller in the 10-mb scenario

because it typically experiences a larger number of scatterings. Figure 2c shows the average energy loss of charm quarks as a function of their momentum. These values are expected to be similar in the range of $\sigma = 3$–10 mb, and their difference is due to the probability distribution of $N_{\text{scattering}}$. The $\langle \Delta E \rangle$ increases as the momentum of the charm quark increases, and its value is close to that of the calculation based on a linearized Boltzmann transport model [20].

2.3 Two-particle angular correlation

To study the azimuthal angle dependence of the charm evolution in hot dense medium simulated in AMPT, two-particle angular correlations are used, which is a powerful tool to determine the interaction of the lower energy jet (or parton) with the surrounding medium. The analysis process is described in detail in Refs. [31–34], and we briefly introduce the method in this section. Selected particles from each event are paired for correlations as

$$S(\Delta\eta, \Delta\phi) = \frac{\mathrm{d}^2 N_{\text{pairs}}^{\text{signal}}}{\mathrm{d}\Delta\eta \mathrm{d}\Delta\phi}, \tag{1}$$

while they are combined with particles from different events to build the background distribution

$$B(\Delta\eta, \Delta\phi) = \frac{\mathrm{d}^2 N_{\text{pairs}}^{\text{mixed}}}{\mathrm{d}\Delta\eta \mathrm{d}\Delta\phi}, \tag{2}$$

where $\Delta\phi$ is the relative azimuthal angle and $\Delta\eta$ is the relative pseudorapidity between the particle pair. In our analysis, each event is mixed with ten other events to improve the statistical power of the background estimation, while the direction of the impact parameter of the collisions in the AMPT events is rotated randomly in the transverse plane to calculate $B(\Delta\eta, \Delta\phi)$. Then, the two-particle correlation function can be obtained as
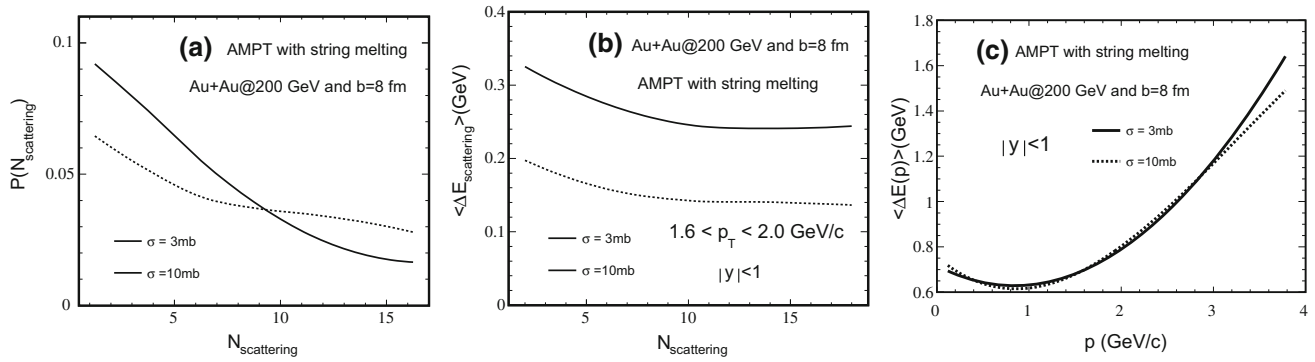
Fig. 2 a Normalized probability distributions of charm quark freezing-out after $N_{scattering}$ collisions in AMPT with cross sections of 3 mb and 10 mb, respectively. **b** Corresponding average energy loss of charm quarks with initial transverse momentum of $1.6 < p_T < 2.0$ GeV/c as a function of their number of collisions in ZPC. **c** Average energy loss of charm quarks in different momentum windows

$$C(\Delta\eta, \Delta\phi) = \frac{S(\Delta\eta, \Delta\phi)}{B(\Delta\eta, \Delta\phi)} \times \frac{N_{pairs}^{mixed}}{N_{pairs}^{signal}}. \tag{3}$$

A one-dimensional $\Delta\phi$ correlation function can be constructed from the $C(\Delta\eta, \Delta\phi)$ by integrating over $\Delta\eta$ as

$$C(\Delta\phi) = A \times \frac{\int S(\Delta\eta, \Delta\phi)d\Delta\eta}{\int B(\Delta\eta, \Delta\phi)d\Delta\eta}, \tag{4}$$

where the normalization constant A is given by $N_{pairs}^{mixed}/N_{pairs}^{signal}$. The distribution of pairs in $\Delta\phi$ can be expanded to a Fourier series,

Fig. 3 (Color online) Elliptic flow v_2 of mid-rapidity hadrons as a function of p_T in 0–80% Au + Au collisions at $\sqrt{s_{NN}} = 200$ GeV. The calculations were performed with total parton cross sections of 3 and 10 mb. The experimental data were obtained from Refs. [4, 35]
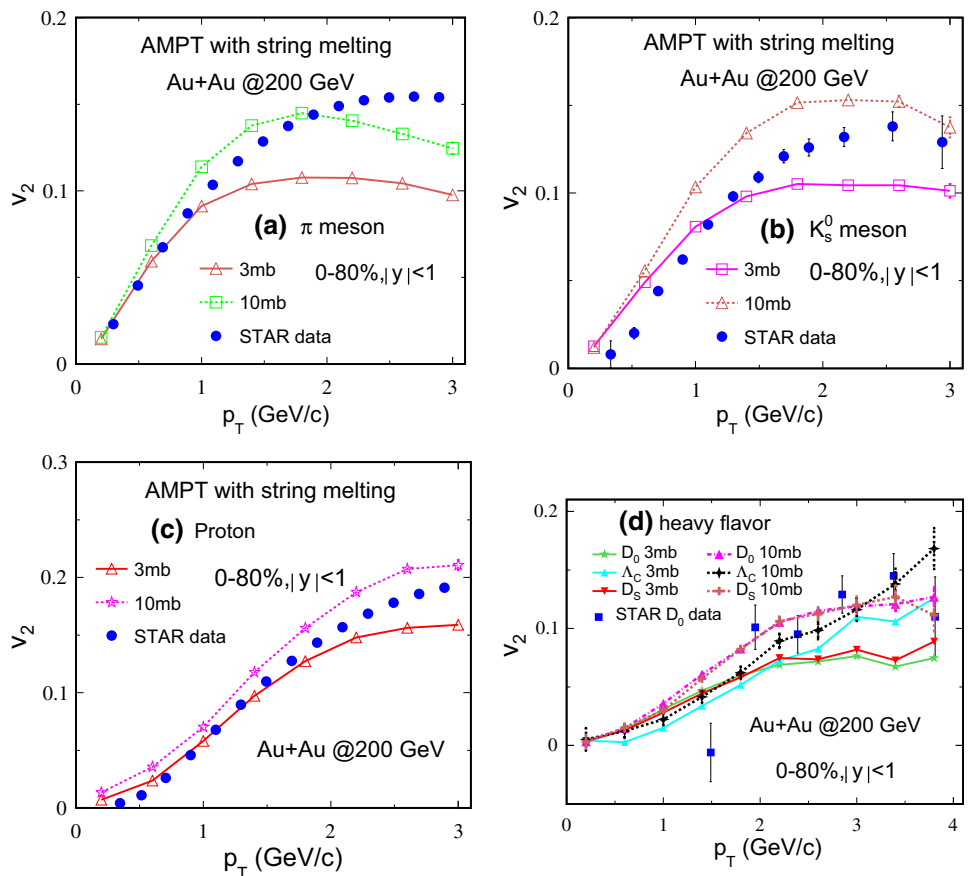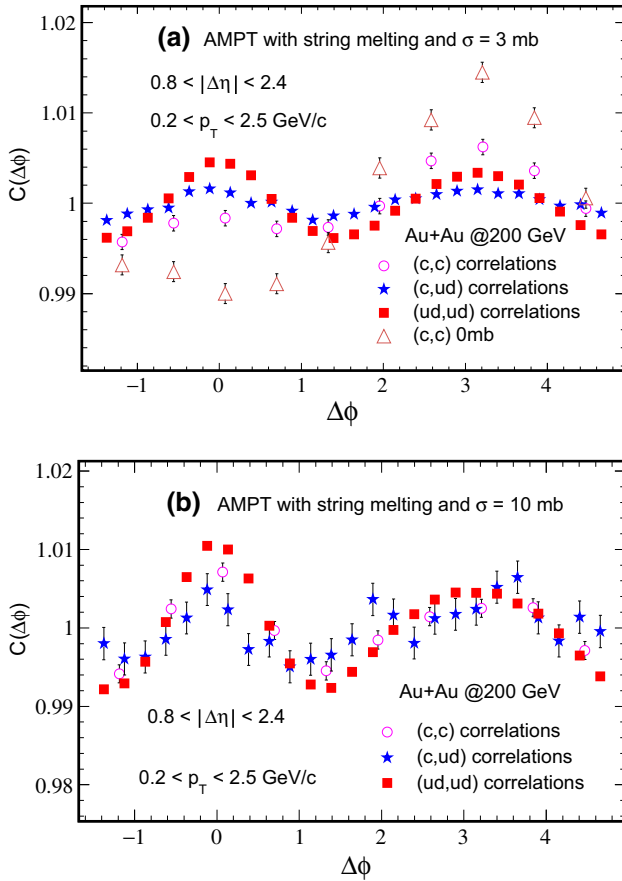
Fig. 4 (Color online) Two-particle azimuthal correlations between charm quarks (open symbols), charm quarks and light quarks (blue stars), and light quarks (red squares) in 0–80% Au + Au collisions at $\sqrt{s_{NN}} = 200$ GeV from AMPT: the total parton cross section of 3 mb (**a**) and 10 mb (**b**). A scenario of charm–charm azimuthal correlations without parton interaction is also shown in (**a**)

$$\frac{dN_{\text{pairs}}}{d\Delta\phi} \propto 1 + 2\sum_{n=1}^{\infty} v_{n,n}(p_T^1, p_T^2)\cos(n\Delta\phi). \tag{5}$$

The coefficients $v_{n,n}$ can be directly calculated by

$$v_{n,n} = \langle\cos(n\Delta\phi)\rangle = \frac{\sum_{m=1}^{N}\cos(n\Delta\phi_m)C(\Delta\phi_m)}{\sum_{m=1}^{N}C(\Delta\phi)}, \tag{6}$$

where $n = 2, 3, 4$ and $N = 200$ is the number of $\Delta\phi$ bins. The harmonic flow coefficients $v_n(n = 2, 3, 4)$ can be calculated as $v_n = v_{n,n}/\sqrt{|v_{n,n}|}$.

2.4 Azimuthal correlation of charm quarks and charm hadrons

The azimuthal anisotropy of charm and light hadrons can be obtained from the two-particle angular correlations as described above. Figure 3 shows the elliptic flow v_2 of mid-rapidity hadrons as a function of p_T in 0–80% Au + Au collisions at $\sqrt{s_{NN}} = 200$ GeV, for πs (Fig. 3a), K_S^0s
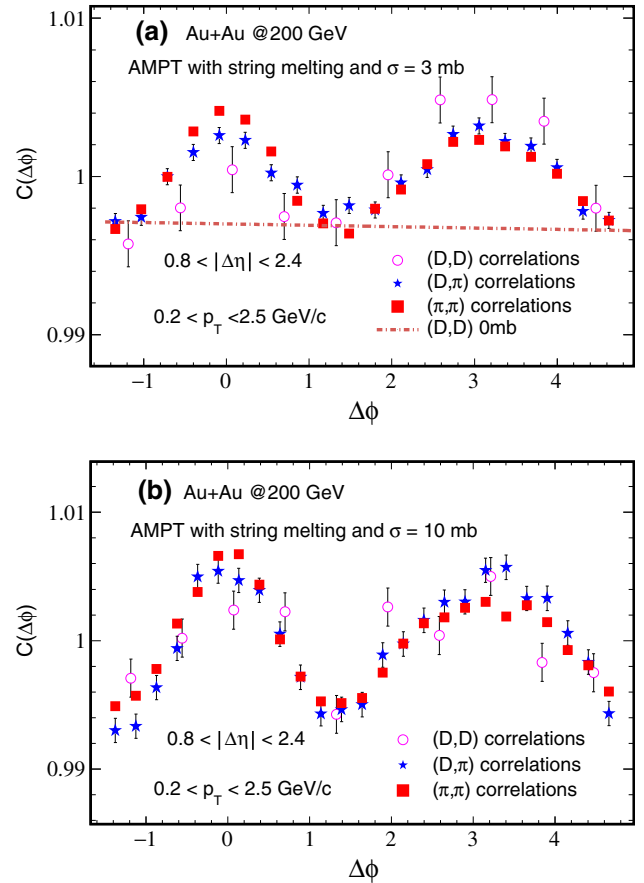
Fig. 5 (Color online) Two-particle azimuthal correlations of D–D, D–π, and π–π in 0–80% Au + Au collisions at $\sqrt{s_{NN}} = 200$ GeV from AMPT: total parton cross section of 3 mb (**a**) and 10 mb (**b**). A scenario of D–D correlations without parton interaction is plotted for reference in panel (**a**)

(Fig. 3b), protons (Fig. 3c), and charm hadrons (Fig. 3d). Systematically, the AMPT model calculations with a parton cross section of 3 mb generate a smaller elliptic flow than those from 10 mb, and they describe the low p_T data better than results from 10 mb, as shown in Fig. 3. When p_T increases to 1.5 GeV/c and above, results from the AMPT model with a parton cross section of 3 mb underestimate the data. From this p_T range, results from the AMPT model with a parton cross section of 10 mb are closer to the data. As shown in Fig. 2, results in the range of 3–10 mb represent the different number of parton collisions and they are responsible for the difference in the v_2 values. This is also the case for charm hadrons (cf. Fig. 2d). For the D hadron result, as data are only available from $p_T > 1.0$ GeV/c, the AMPT result with a cross section of 10 mb gives better description of the D_0 data. Calculations on Λ_c and D_s are also available. They follow a similar p_T and parton cross-sectional dependence behavior as those other particles presented in panels (a–d) of Fig. 3. Further measurements of the elliptic flow of Λ_c and D_s at

RHIC energies can help to distinguish the parton cross-sectional dependence of $v_2(p_T)$ behavior.

Then, the charm–charm azimuthal correlations were studied in Au + Au collisions at $\sqrt{s_{NN}} = 200$ GeV. Figure 4 shows the quarks azimuthal correlations, which was performed at the stage of parton freeze-out in ZPC, prior to the hadronization in AMPT. Partons with $p_T < 2.5$ GeV/c were chosen to cover the majority of quarks in the collisions, which required a η gap of (0.8,2.4) between quarks. It should be noted that the kinematic window needs to be adjusted with different acceptance in different experiments. In the case of the total parton cross section of 3 mb (Fig. 4a), the charm–charm correlation is suppressed at the near side and enhanced at the far side, which is different from the distributions of light quark azimuthal correlations. This is possibly due to a stronger effect of the initial production on the massive charm quarks, as indicated by the open triangles in Fig. 4 and discussed in Ref. [36]. The increase in the total parton cross section enhances the collision probability among quarks (cf. Fig. 2); thus, it reduces the difference from the effect of initial production between the charm and light quarks. This is shown in Fig. 4b, with a larger total parton cross-sectional calculation, where the correlations between the charm quarks are nearly the same as light quarks.

These charm quarks coalesce into a charm hadron with the nearby quarks and undergo hadronic interaction in the AMPT. Figure 5 shows the corresponding charm hadron azimuthal correlations together with light hadrons. In the case of the total parton cross section of 3 mb, the correlations between D–π are nearly identical to those of π–π, suggesting hadronization and hadronic scattering effect on the evolution of charm hadrons, while the correlations between D–D are slightly different from those of light hadrons. They have a slightly higher distribution on the far side and a lower distribution on the near side. According to the study with the larger total parton cascade cross section of 10 mb (panel Fig. 4b), the correlations between charm hadrons and between light hadrons are the same. Figure 5a shows a calculation of D–D correlations without parton interaction (the 0-mb cross-sectional scenario), which gives a flat distribution along $\Delta\phi$. This is a scenario with hadronization and hadronic interaction only, which is similar to the default version of the AMPT model. The comparison of D–D azimuthal correlations among different parton cross-sectional parameters applied in AMPT suggests that the number of parton collisions affects the evolution of charm quarks in QGP medium.

We also studied the high p_T charm hadron azimuthal correlations in QGP medium. Figure 6 shows the two-particle azimuthal correlations with a trigger particle $p_T > 5$ GeV/c and its associated particle at $p_T < 2$ GeV/c.
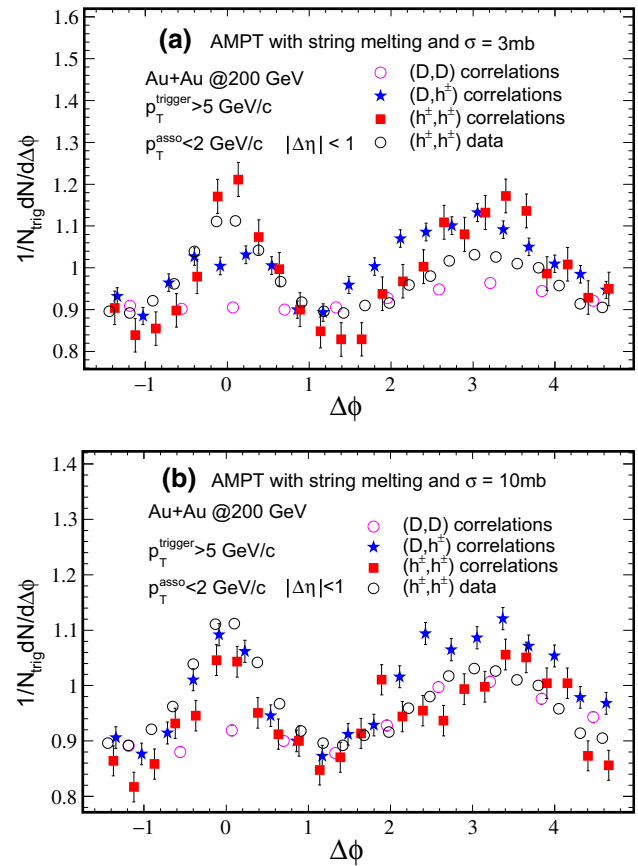

Fig. 6 (Color online) The two-particle azimuthal correlations of D–D, D–$h^{\pm}$, and $h^{\pm}$–$h^{\pm}$ in 0–80% Au + Au collisions at $\sqrt{s_{NN}} = 200$ GeV, with a trigger particle of $p_T > 5$ GeV/c and associated particle of $p_T < 2$ GeV/c. Experimental data on charge hadron azimuthal correlation are obtained from Ref. [37]

The correlations are normalized with respect to the number of triggers. The results of charge hadron azimuthal correlations from AMPT partially describe the experimental data, which are slightly different in parton cross sections of 3 and 10 mb, because only elastic scattering is included in the current calculations. For the D–D correlations with small parton cross section, similar to the low p_T azimuthal correlation results, shown in of Fig. 5a, the high p_T D–D correlations exhibit different behavior than the light flavor charge hadrons, in this case with lower yield on both the near and far sides. For the case of 10-mb parton cross section, correlations between D–D are similar to light charge hadrons on the far side, and lower on the near side, as shown in Fig. 5b.

3 Summary

We studied the charm quark evolution in QGP medium created in ultrarelativistic heavy ion collisions with the AMPT model. By including an additional $c\bar{c}$ production in

the AMPT to reproduce the open charm hadron p_T spectrum in 0–80% Au + Au collisions at $\sqrt{s_{NN}} = 200$ GeV, we obtained a reasonable description of the elliptic flow of the D meson, and then predictions were provided for other charm hadrons including D_s, Λ_c, and J/ψ. We also studied the azimuthal angular correlations between D mesons. We found that the total parton cross section presents a clear effect on the D meson azimuthal correlations. By combining the different charm quark average energy loss with different parton cascade cross-section parameters, our studies provide an effective method to understand the collisional energy loss of charm quarks in hot QGP medium. Therefore, further experimental measurements from LHC and sPHENIX are required.

References

1. E. Shuryak, Strongly coupled quark–gluon plasma in heavy ion collisions. Rev. Mod. Phys. **89**, 035001 (2017). https://doi.org/10.1103/RevModPhys.89.035001

2. J.H. Chen, D. Keane, Y.G. Ma et al., Antinuclei in heavy-ion collisions. Phys. Rep. **760**, 1 (2018). https://doi.org/10.1016/j.physrep.2018.07.002

3. H.C. Song, Y. Zhou, K. Gajdosova, Collective flow and hydrodynamics in large and small systems at the LHC. Nucl. Sci. Tech. **28**, 99 (2017). https://doi.org/10.1007/s41365-017-0245-4

4. L. Adamczyk, J.K. Adkins, G. Agakishiev et al., Measurement of D0 azimuthal anisotropy at midrapidity in Au + Au collisions at $\sqrt{s_{NN}} = 200$ GeV. Phys. Rev. Lett. **118**, 212301 (2017). https://doi.org/10.1103/PhysRevLett.118.212301

5. X.Dong, Y.J. Lee, R. Rapp, Open heavy-flavor production in heavy-ion collisions. arXiv:1903.07709

6. S.S. Cao, G. Coci, S.K. Das et al., Toward the determination of heavy-quark transport coefficients in quark–gluon plasm. Phys. Rev. C **99**, 054907 (2019). https://doi.org/10.1103/PhysRevC.99.054907

7. A. Andronic, F. Arleo, R. Arnaldi et al., Heavy-flavour and quarkonium production in the LHC era: from proton–proton to heavy-ion collisions. Eur. Phys. J. C **76**, 107 (2016). https://doi.org/10.1140/epjc/s10052-015-3819-5

8. H. Hees, V. Greco, R. Rapp, Heavy-quark probes of the quark–gluon plasma and interpretation of recent data taken at the BNL Relativistic Heavy Ion Collider. Phys. Rev. C **73**, 034913 (2006). https://doi.org/10.1103/PhysRevC.73.034913

9. P.B. Gossiaux, R. Bierkandt, J. Aichelin, Tomography of quark gluon plasma at energies available at the BNL Relativistic Heavy Ion Collider (RHIC) and the CERN Large Hadron Collider (LHC). Phys. Rev. C **79**, 044906 (2016). https://doi.org/10.1103/PhysRevC.79.044906

10. M. He, R.J. Fries, R. Rapp, Heavy-quark diffusion and hadronization in quark–gluon plasma. Phys. Rev. C **86**, 014903 (2012). https://doi.org/10.1103/PhysRevC.86.014903

11. S. Plumari, V. Minissale, S.K. Das et al., Charmed hadrons from coalescence plus fragmentation in relativistic nucleus–nucleus collisions at RHIC and LHC. Eur. Phys. J. C **78**, 348 (2018). https://doi.org/10.1140/epjc/s10052-018-5828-7

12. S.S. Adler, S. Afanasiev, C. Aidala et al., Nuclear modification of electron spectra and implications for heavy quark energy loss in Au + Au collisions at $\sqrt{s_{NN}} = 200$ GeV. Phys. Rev. Lett. **96**, 032301 (2006). https://doi.org/10.1103/PhysRevLett.96.032301

13. A. Adare, S. Afanasiev, C. Aidala et al., Energy loss and flow of heavy quarks in Au + Au collisions at $\sqrt{s_{NN}} = 200$ GeV. Phys. Rev. Lett. **98**, 172301 (2007). https://doi.org/10.1103/PhysRevLett.98.172301

14. B.I. Abelev, M.M. Aggarwal, Z. Ahammed et al., Transverse momentum and centrality dependence of high-pT nonphotonic electron suppression in Au + Au collisions at $\sqrt{s_{NN}} = 200$ GeV. Phys. Rev. Lett. **98**, 192301 (2007). https://doi.org/10.1103/PhysRevLett.98.192301

15. A. Buzzatti, M. Gyulassy, Jet flavor tomography of quark gluon plasmas at RHIC and LHC. Phys. Rev. Lett. **108**, 022301 (2012). https://doi.org/10.1103/PhysRevLett.108.022301

16. B. Abelev, J. Adam, D. Adamova et al., Suppression of high transverse momentum D mesons in central Pb–Pb collisions at $\sqrt{s_{NN}} = 2.76$ TeV. J. High Energy Phys. **2012**, 112 (2012). https://doi.org/10.1007/JHEP09(2012)112

17. B. Abelev, J. Adam, D. Adamova et al., D meson elliptic flow in noncentral Pb–Pb collisions at $\sqrt{s_{NN}} = 2.76$ TeV. Phys. Rev. Lett. **111**, 102301 (2013). https://doi.org/10.1103/PhysRevLett.111.102301

18. L. Adamczyk, J.K. Adkins, G. Agakishiev et al., Observation of D0 meson nuclear modifications in Au + Au collisions at $\sqrt{s_{NN}} = 200$ GeV. Phys. Rev. Lett. **113**, 142301 (2014). https://doi.org/10.1103/PhysRevLett.113.142301

19. A. Adare, C. Aidala, N.N. Ajitanand et al., Heavy-quark production and elliptic flow in Au + Au collisions at $\sqrt{s_{NN}} = 62.4$ GeV. Phys. Rev. C **91**, 044907 (2015). https://doi.org/10.1103/PhysRevC.91.044907

20. S.S. Cao, T. Luo, G.Y. Qing et al., Linearized Boltzmann transport model for jet propagation in the quark–gluon plasma: heavy quark evolution. Phys. Rev. C **94**, 014909 (2016). https://doi.org/10.1103/PhysRevC.94.014909

21. M. He, R.J. Fries, R. Rapp, Heavy flavor at the large hadron collider in a strong coupling approach. Phys. Lett. B **735**, 445 (2014). https://doi.org/10.1016/j.physletb.2014.05.050

22. Z.W. Lin, C.M. Ko, B.A. Li et al., Multiphase transport model for relativistic heavy ion collisions. Phys. Rev. C **72**, 064901 (2005). https://doi.org/10.1103/PhysRevC.72.064901

23. AMPT source codes are available at http://myweb.ecu.edu/linz/ampt/. Accessed 10 Apr 2015

24. X.N. Wang, M. Gyulassy, HIJING: a Monte Carlo model for multiple jet production in pp, p A, and A A collisions. Phys. Rev. D **44**, 3501 (1991). https://doi.org/10.1103/PhysRevD.44.3501

25. http://home.thep.lu.se/~torbjorn/Pythia.html. Accessed 1 Apr 2001

26. B. Zhang, Erratum to "ZPC 1.0.1" a parton cascade for ultrarelativistic heavy ion collisions. Comput. Phys. Commun. **109**, 193–206 (1998). https://doi.org/10.1016/S0010-4655(98)00010-1

27. B.A. Li, C.M. Ko, Formation of superdense hadronic matter in high energy heavy-ion collisions. Phys. Rev. C **52**, 2037 (1995). https://doi.org/10.1103/PhysRevC.52.2037

28. L. Adamczyk, J.K. Adkins, G. Agakishiev et al., J/Ψ production at low pT in Au + Au and Cu+Cu collisions at $\sqrt{s_{NN}} = 200$ GeV with the STAR detector. Phys. Rev. C **90**, 024906 (2014). https://doi.org/10.1103/PhysRevC.90.024906

29. C. Zhang, L. Zheng, F. Liu et al., Update of a multiphase transport model with modern parton distribution functions and nuclear shadowing. Phys. Rev. C **99**, 064906 (2019). https://doi.org/10.1103/PhysRevC.99.064906

30. L. He, T. Edmonds, Z.W. Lin et al., Anisotropic parton escape is the dominant source of azimuthal anisotropy in transport models.

Phys. Lett. B **753**, 506 (2016). https://doi.org/10.1016/j.physletb.2015.12.051

31. G. Aad, B. Abbott, J. Abdallah et al., Measurement of the azimuthal anisotropy for charged particle production in $\sqrt{s_{NN}} = 2.76$ TeV lead–lead collisions with the ATLAS detector. Phys. Rev. C **86**, 014907 (2012). https://doi.org/10.1103/PhysRevC.86.014907

32. S. Chatrchyan, V. Khachatryan, A.M. Sirunyan et al., Multiplicity and transverse momentum dependence of two- and four-particle correlations in pPb and PbPb collisions. Phys. Lett. B **724**, 213 (2013). https://doi.org/10.1016/j.physletb.2013.06.028

33. L.Y. Zhang, J.H. Chen, Z.W. Lin et al., Two-particle angular correlations in pp and p-Pb collisions at energies available at the CERN Large Hadron Collider from a multiphase transport model. Phys. Rev. C **98**, 034912 (2018). https://doi.org/10.1103/PhysRevC.98.034912

34. L.Y. Zhang, J.H. Chen, Z.W. Lin et al., Two-particle angular correlations in heavy ion collisions from a multiphase transport model. Phys. Rev. C **99**, 054904 (2019). https://doi.org/10.1103/PhysRevC.99.054904

35. L. Adamczyk, J.K. Adkins, G. Agakishiev et al., Centrality and transverse momentum dependence of elliptic flow of multistrange hadrons and ϕ meson in Au + Au collisions at $\sqrt{s_{NN}} = 200$ GeV. Phys. Rev. Lett. **116**, 062301 (2016). https://doi.org/10.1103/PhysRevLett.116.062301

36. X. Zhu, N. Xu, P. Zhuang, Effect of partonic wind on charm quark correlations in high-energy nuclear collisions. Phys. Rev. Lett. **100**, 152301 (2008). https://doi.org/10.1103/PhysRevLett.100.152301

37. A. Adare et al., Measurement of two-particle correlations with respect to second- and third-order event planes in Au + Au collisions at $\sqrt{s_{NN}} = 200$ GeV. Phys. Rev. C **99**, 054903 (2019). https://doi.org/10.1103/PhysRevC.99.054903